ResearchGate

See discussions, stats, and author profiles for this publication at: https://www.researchgate.net/publication/235657481

Cellulose Microfibril Twist, Mechanics, and Implication for Cellulose Biosynthesis

ARTICLE *in* THE JOURNAL OF PHYSICAL CHEMISTRY A · FEBRUARY 2013

Impact Factor: 2.69 · DOI: 10.1021/jp3089929 · Source: PubMed

CITATIONS
16

READS
72

7 AUTHORS, INCLUDING:

Zhen Zhao
Pennsylvania State University
4 PUBLICATIONS **35** CITATIONS
SEE PROFILE

Oleg E Shklyaev
Pennsylvania State University
16 PUBLICATIONS **123** CITATIONS
SEE PROFILE

Mohamed Naseer ali Mohamed
The New College
15 PUBLICATIONS **149** CITATIONS
SEE PROFILE

J. D. Kubicki
University of Texas at El Paso
215 PUBLICATIONS **4,433** CITATIONS
SEE PROFILE

Available from: Mohamed Naseer ali Mohamed
Retrieved on: 26 January 2016

THE JOURNAL OF PHYSICAL CHEMISTRY A

Article

pubs.acs.org/JPCA

Cellulose Microfibril Twist, Mechanics, and Implication for Cellulose Biosynthesis

Zhen Zhao,[†] Oleg E. Shklyaev,[†,§] Abdolmajid Nili,[†,§] Mohamed Naseer Ali Mohamed,[†,‡,⊥] James D. Kubicki,[†,‡] Vincent H. Crespi,[†,§] and Linghao Zhong*[,†,∥]

[†]Center for Lignocellulose Structure and Formation, Pennsylvania State University, State College, Pennsylvania 16801, United States

[‡]Department of Geosciences, Pennsylvania State University, State College, Pennsylvania 16801, United States

[§]Departments of Physics, Chemistry, and Materials Science and Engineering, The Pennsylvania State University, State College, Pennsylvania 16801, United States

[∥]Department of Chemistry, Pennsylvania State University, Mont Alto, Pennsylvania 17237, United States

Supporting Information

ABSTRACT: All-atom molecular dynamics simulations with explicit water solvent were used to investigate the microstructure and conformational dynamics of cellulose Iβ microfibrils as a function of microfibril length and cross-sectional size and shape. Cellulose microfibrils quickly develop a right-handed twist, which then remains stable over the entire 10 ns simulation time. The helical angle is independent of microfibril length and inversely proportional to its cross-sectional area, in accord with the expectations of continuum theory for an intrinsic chiral twist that is opposed by torsional shear. These calculations provide—to our knowledge—the first estimates of the shear modulus of a cellulose microfibril from MD simulations. The internal strains caused by this helical twist, propagated indefinitely along the microfibril axis, could be relaxed by periodic regions of amorphous structure along the axis of the cellulose microfibrils.

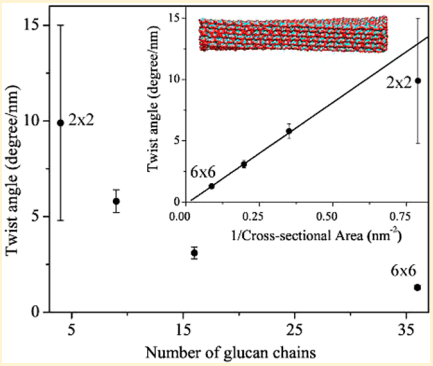

I. INTRODUCTION

Cellulose, the most abundant biopolymer, has been a ubiquitous raw material since ancient times. Advanced applications of cellulose in biofuel and materials have been attracting increasing attention, but these applications are hindered by difficulties in cellulose extraction due to cell wall recalcitrance, as well as the inefficient cellulose degradation process. A more complete fundamental understanding of the driving forces behind cellulose microstructure could assist in guiding efforts toward more efficient cellulose usage.

Cellulose is a linear polysaccharide of β-(1−4)-linked D-glucan units, as shown in Figure 1. It forms microfibrils upon biosynthesis. In higher plants, approximately 24−36 individual glucan chains assemble into units commonly named elementary fibrils, or microfibrils.[1] These cellulose microfibrils then assemble into larger units, which in turn pack into cellulose fibers. Although cellulose from different sources may pack differently, these microfibrils generally have diameters from 2 to 4 nm, as revealed by X-ray small-angle scattering and electron microscopy.[2−9] The relative uniformity of the observed cellulose microfibril diameter suggests a general mechanism governing fiber diameter (independent of the process by which thicker bundles form via aggregation of microfibrils).

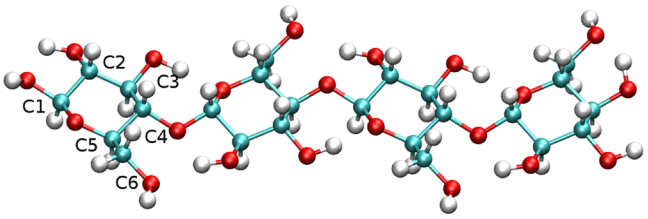

Figure 1. The structure of a cellulose chain. The names of carbon atoms are marked.

The structures of cellulose Iβ, Iα, II, and III have been determined by crystallography and neutron diffraction.[10−16] In these structure determinations, the glucan chain is assumed to be flat, so that the cellulose crystallite as a whole is straight (i.e., not twisted). In computer simulations with Hartree−Fock and density functional theory,[17−21] a 180° turn is observed for the glycosidic linkage between glucose units; thus, these results confirmed the nontwisted structure of cellobiose. However, small molecular models were used in these calculations, and they do not capture the chiral interchain interactions within a microfibril as a whole. Certain experimental evidence suggests that cellulose microfibrils are twisted. Hanley and Gray reported a right-handed helical twist for microfibrils from *M. denticulata* using atomic force microscopy and transmission electron microscopy.[22] Narrow twisted ribbons of cellulose

Received: September 10, 2012
Revised: February 15, 2013
Published: February 18, 2013

 © 2013 American Chemical Society dx.doi.org/10.1021/jp3089929 | *J. Phys. Chem. A* 2013, 117, 2580−2589

were observed during biosynthesis of bacterial cellulose.[23−44] Left-handed helical microfibrils have been reported for primary plant wall cellulose.[45] These experimental observations are also backed by some theoretical investigations. Several groups[46−51] independently reported molecular dynamics studies of large, solvated cellulose Iβ/Iα/III_I systems. The glycosidic linkage is slightly off from 180° in these MD simulations, leading to gently twisted microfibrils. More interestingly, Matthews et al. later found that a twisted cellulose microfibril untwists itself when their molecular dynamics simulations were extended for a much longer time at both high[52] and low[53] temperatures. The goal of our study is not to contribute specifically to the twisted-versus-nontwisted debate. Instead, our focus is to study the properties of cellulose microfibrils when they are in a twisted state—the existence of which has been supported by many microscopic studies.

In a twisted cellulose microfibril, surface chains travel longer distances than those close to the center. Thus, in order to maintain crystalline registry between neighboring chains, the system must develop inhomogeneous axial strain, supported by the shear strength of the interchain supramolecular interactions. In a sufficiently wide microfibril, this axial strain could exceed the binding free energy of the chain to the remainder of the fibril, at which point it would become unfavorable for further chains to adhere to the microfibril with periodic axial registry (i.e., in the strained state). A similar limiting mechanism has been proposed to control the diameter of fibrin, sickle cell hemoglobin aggregates, and nanostructures of silica rods within ordered mesopores.[54−56] Beyond the possibility of cellulose microfibril twist, small angle neutron scattering on cellulose fibers from ramie and *Populus maximowicii* (cotton wood) showed periodic disordered regions along the fibers, with 4−5 disordered residues every ∼300 residues.[57] A pronounced deviation from crystalline registry across the cross section of the microfibril would release the accumulated shear strain due to crystalline twist.

In this study, cellulose elementary fibrils with different lengths and different cross-sectional areas and shapes, all based on the cellulose Iβ crystal structure, have been studied by all-atom molecular dynamics in explicit solvent. The microfibrils quickly develop a right-handed twist during the early stages of each simulation, and this twist remains stable for the remainder of the 10 ns molecular dynamics run. For the first time, our results reveal a clear relation between cellulose microfibril geometry and twist microstructure. The wider the cellulose microfibril, the smaller the helical angle (helical angle is defined as the angle twisted per unit axial distance), with the angle precisely inversely proportional to the microfibril's cross-sectional area. Furthermore, the helical angle is found to be independent of microfibril length. Artificial reduction of the stiffness of the glycosidic bond has a very limited effect on the helical angle, demonstrating that the extensional stiffness of the chain is not the force that counterbalances intrinsic twist. Instead, the precise inverse-area scaling of twist angle suggests that the fibril's torsional stiffness plays this role. Within the MD simulations, twist appears to be an intrinsic property of cellulose microfibrils.

II. METHODS

On the basis of the known crystal structure of cellulose Iβ reported by Nishiyama et al.[10] from X-ray fiber diffraction analysis of crystallized tunicate cellulose, we generated several atomistic models of cellulose microfibrils. The unit cell was reported to be monoclinic (space group *P*21) and consisted of the two molecules (labeled as "origin" and "center") shown in Figure 2. To construct a microfibril, this crystal structure must

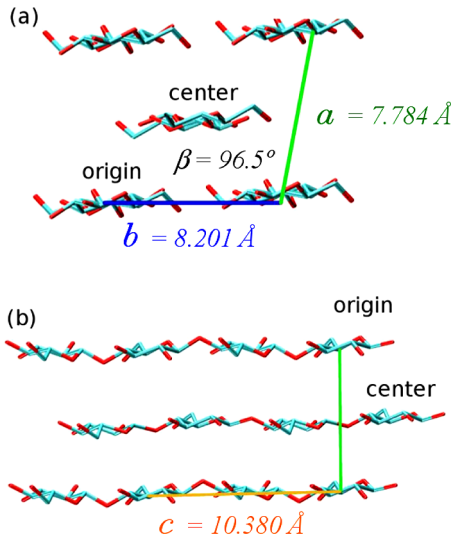

Figure 2. The unit cell of cellulose Iβ, hydrogen atoms omitted for clarity, as viewed (a) down the *c*-axis and (b) down the *b*-axis.

be truncated at the microfibril surface. The "square" microfibril of Figure 3e is terminated along the (100) and (010) planes.

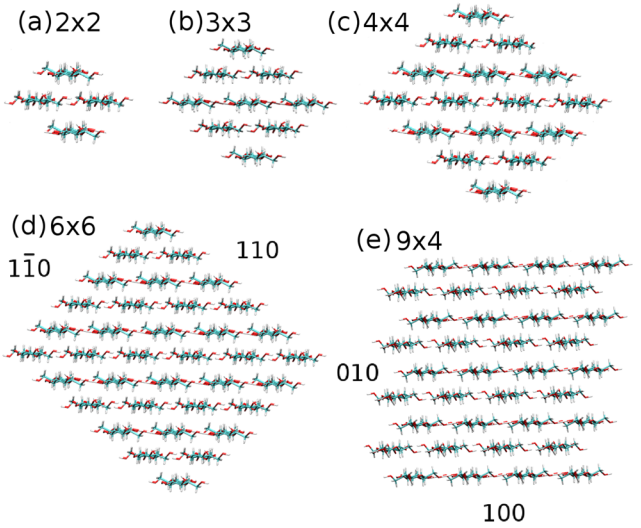

Figure 3. Various cellulose microfibril models considered in this study: (a) 2 × 2, (b) 3 × 3, (c) 4 × 4, and (d) 6 × 6 diagonal microfibrils and (e) 9 × 4 square microfibril.

Due to the low monoclinic symmetry, the (010) termination, although low index, is rough. The rough (010) surface has dangling hydrogen bonds and hence is more hydrophilic compared to the (100) plane, which presents a relatively smooth hydrophobic surface. We also consider a "diagonal" truncation which terminates the fibril along the (110) and (1$\bar{1}$0) planes, as shown in Figure 3a−d. These faces contain many hydroxymethyl groups and are hydrophilic. These models thus emphasize different crystal faces. The chains in diagonal microfibrils are all 40 glucose units in length, while the square microfibrils vary from 20 to 40 monomer units in length. The lateral width ranges from 1 to 5 nm.

dx.doi.org/10.1021/jp3089929 | J. Phys. Chem. A 2013, 117, 2580−2589

All simulations are performed with CHARMM,[58] using parameters developed for carbohydrates[59,60] which have reproduced a variety of experimental properties including crystal cell parameters and intramolecular geometries, aqueous densities, and aqueous NMR coupling constants for monosaccharides and disaccharides. Each cellulose microfibril model is centered in a box of explicit TIP3P water molecules[61,62] with a solvation shell of at least 10 Å for each atom in the microfibril. Long-range electrostatics is handled using the particle-mesh Ewald algorithm with a 1 Å charge grid size. Nonbonded interactions are truncated at 10 Å. All chemical bonds involving H atoms are fixed in length by the SHAKE algorithm.[63] First, 100 steps of steepest descent are followed by 100 steps of conjugate gradient minimization to relieve any large strains associated with the initial conditions. The system is then prepared by a stepwise heating at 100, 200, and 300 K, holding for 10 ps at each stage, followed by a 20 ps equilibration at 300 K. The 10 ns production trajectory is collected in the NVE ensemble using a Verlet integrator with a step size of 1 fs. Configurations are saved every 0.1 ps for later analysis.

III. RESULTS AND DISCUSSION

3.1. Atomic-Level Structure of Cellulose Microfibrils.

3.1.1. Overall Microfibril Stability. Table 1 summarizes the average unit-cell dimensions for the 3 × 3, 6 × 6, and 9 × 4 microfibrils. The parameters are calculated for the central core chains, averaged over the last 1 ns of each MD trajectory. The fluctuation of the 2 × 2 microfibril is so large that no order can be found at the end of the 10 ns MD; thus, its unit cell parameters are meaningless and are not included. In general, the average unit-cell dimensions obtained from the simulation are in good agreement (difference <2.5%) with the diffraction studies. The 6 × 6 and 9 × 4 models have very similar unit-cell dimensions (<0.2%). For microfibrils with a smaller cross-sectional area (3 × 3), we observe a more relaxed intersheet structure, indicated by an increase in the unit cell parameters *a* and *β* (2.2% increase for *a* and 1.3% increase for *β* compared with the 6 × 6 model). Also, we observe larger fluctuations in unit-cell dimensions in smaller-diameter fibrils.

Table 1. Unit Cell Dimension of Cellulose Iβ Microfibril from X-ray Diffraction[10] and from MD Simulation (Average over Last 1 ns)

	X-ray[10]	3 × 3 model	4 × 4 model	6 × 6 model
a (Å)	7.78	7.85 ± 0.24	7.68 ± 0.19	7.69 ± 0.19
b (Å)	8.20	8.28 ± 0.16	8.33 ± 0.12	8.32 ± 0.15
c (Å)	10.38	10.44 ± 0.09	10.46 ± 0.09	10.47 ± 0.09
β (deg)	96.5	98.8 ± 2.7	97.5 ± 1.9	97.7 ± 2.1

Our MD simulations show that interactions between glucan chains in adjacent layers, as well as those between neighboring chains in the same layer, lead to the formation of a well-packed core, an important factor for the stability of cellulose microfibrils. The configurations remain compact for both diagonal and square models, including even the 2 × 2 case. Figure 4 shows the root-mean-square deviations in atomic positions across the glucan backbones of a 4 × 4 microfibril (i.e., omitting the C6 hydroxymethyl group and the C2/C3 hydroxyl groups), referenced to the initial ($RMSD_0$), final (i.e., after 10 ns, $RMSD_{10}$), or time-averaged ($RMSD_{ave}$) configurations. Since the orientations of successive unit cells can wander due to long-range deformations of the microfibril, the average structure is obtained by recursive rigid-body alignment followed by averaging until a convergence is achieved. The cellulose microfibril structure relaxes away from the initial crystalline coordinates during the first nanosecond, after which the backbone RMSD settles at ~3.0 Å relative to the starting structure and ~1.0 Å relative to the final structure. $RMSD_{ave}$ (often referred to as RMSF) is similar to $RMSD_{10}$, suggesting that the glucan backbone at 10 ns is very similar to its average.

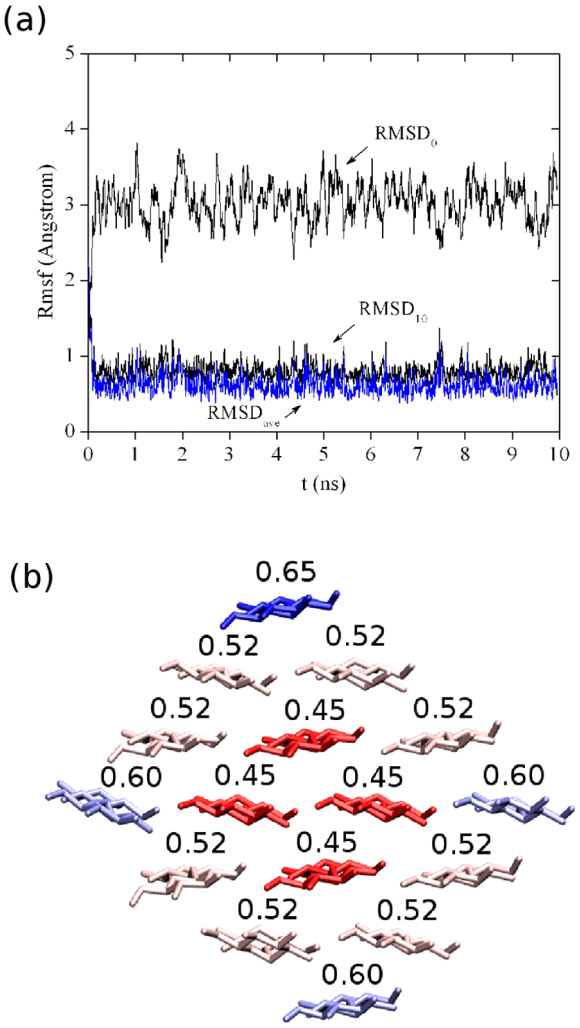

Figure 4. Global and local RMSDs for a 4 × 4 × 40 cellulose microfibril model. (a) RMSD for the backbone atoms of the microfibril over the 10 ns MD simulation time. The starting structure is used as the reference structure for $RMSD_0$, the last MD structure for $RMSD_{10}$, and the average structure over the MD trajectory for $RMSD_{ave}$. $RMSD_{ave}$ is often referred to as RMSF. (b) Color-coded $RMSD_{ave}$ for individual glucan chain (blue for larger values of $RMSD_{ave}$ and red for smaller).

The microfibrils assume a stable conformation with only minor changes of their core structure during the 10 ns of the MD trajectories. The major structural changes in the first nanosecond reflect the formation of a twist about the microfibril axis. The cellulose microfibrils with small cross sections exhibit bigger RMS fluctuations and thus are more structurally disordered, as expected for systems with a larger surface area to volume ratio. For example, $RMSD_{ave}$ is approximately 1.9, 1.0, 0.6, and 0.5 Å for the 2 × 2, 3 × 3, 4 × 4, and 6 × 6 microfibrils, respectively. Figure 4b shows the fluctuations of individual glucan chains as measured by the

dx.doi.org/10.1021/jp3089929 | J. Phys. Chem. A 2013, 117, 2580−2589

RMSDs of chain backbone atoms over the second half of the 10 ns trajectory. The surface regions fluctuate more, especially the corners, which are least constrained by interactions with neighboring chains. This surface disorder is consistent with recent NMR observations[64] which indicated that the interior cellulose is the most rigid polysaccharide in the cell wall. The surface disorder is considered as one form of "amorphous" cellulose.

3.1.2. Observation of Microfibril Twist. The gentle right-handed twist that rapidly develops during initial equilibration remains stable over the life of the simulation. The same cellulose helicity has been observed in many previous classical force field calculations.[46−53] Figure 5a shows a snapshot of the 6 × 6 cellulose microfibril in the surface representation, and the twist is obvious. The helical angle can be extracted from the dihedral angle between the four C1 carbon atoms as joined by the dark lines shown in Figure 5b, measured in units of degrees per nanometer. The twist of each microfibril is stable after the first 1 ns of equilibration, as shown in Figure 5c. We used the last 5 ns of each trajectory for subsequent analysis.

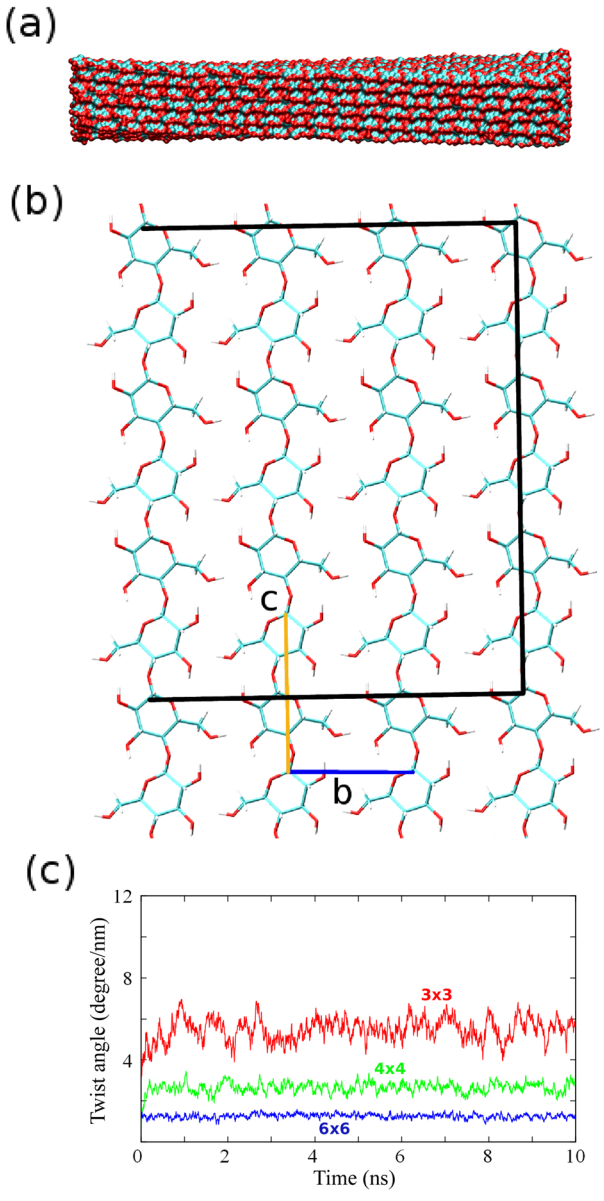

Figure 5. The twist of cellulose microfibril. (a) The final snapshot of the diagonal 6 × 6 cellulose microfibril in surface representation. (b) The helical angle is derived from the dihedral angle of the four C1 carbon atoms indicated by the dark lines. (c) Twist angle profiles for the 3 × 3 (red), 4 × 4 (green), and 6 × 6 (blue) microfibrils over the MD trajectory. The torsional stiffness can be extracted from the fluctuation, as described in the text.

If the twist originates in the intrinsic chirality of the interacting constituent cellobiose subunits within a monoclinic unit cell (and the resulting extensional strains never exceed the shear strength of the microfibril), then the helical angle should be homogeneous along the length of the microfibril, excepting finite-size edge effects near the two ends. Indeed, we find the helical angle remains constant at ∼1.7 ± 0.2°/nm for the 9 × 4 microfibrils of 20, 40, or 60 glucose units in length. The helical angle of individual chains within the microfibril is homogeneous across the cross section (including both center and origin chains), except for the one or two terminal glucose units at both ends of the microfibril. The homogeneous nature of the twist suggests that its origin is intrinsic and distributed uniformly, via a bulk term in the free energy density similar to that seen in chiral liquid crystals.

Since the extensional shear across the radius of a twisted fibril is more severe for wider fibrils (with longer path length differences between the fibril's center and edge), the helical angle should decrease for wider fibrils. Figure 6 confirms this expectation: the helical angle varies from 9.9°/nm for the 2 × 2 microfibril to 5.8, 3.1, and 1.3°/nm for the 3 × 3, 4 × 4, and 6 × 6 microfibrils, respectively (data in the Supporting Information). The "error" bars in Figure 6 represent the fluctuation of the twist over the microfibril (i.e., it is a thermal fluctuation, not a measurement error). The extraordinarily large fluctuation for the 2 × 2 microfibril is due to the loss of structural stability. Therefore, it is excluded in many of the following analyses. The result for the 6 × 6 microfibril agrees with the 1.4°/nm twist obtained by Matthews et al. for a microfibril of the same size and shape but using a different force field.[47]

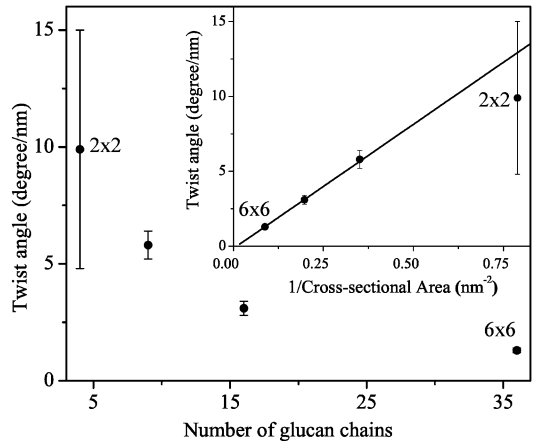

Figure 6. Variation of twist angle of the cellulose microfibril with the number of glucan chains and (inset) with the inverse of microfibril cross-sectional area. The data fitting process can be found in the Supporting Information. The error bar indicates the RMS fluctuations of the twist angle. Due to its large fluctuation, the 2 × 2 microfibril was excluded from the line fitting in the inset, as well as subsequent analysis of mechanical properties.

dx.doi.org/10.1021/jp3089929 | J. Phys. Chem. A 2013, 117, 2580−2589

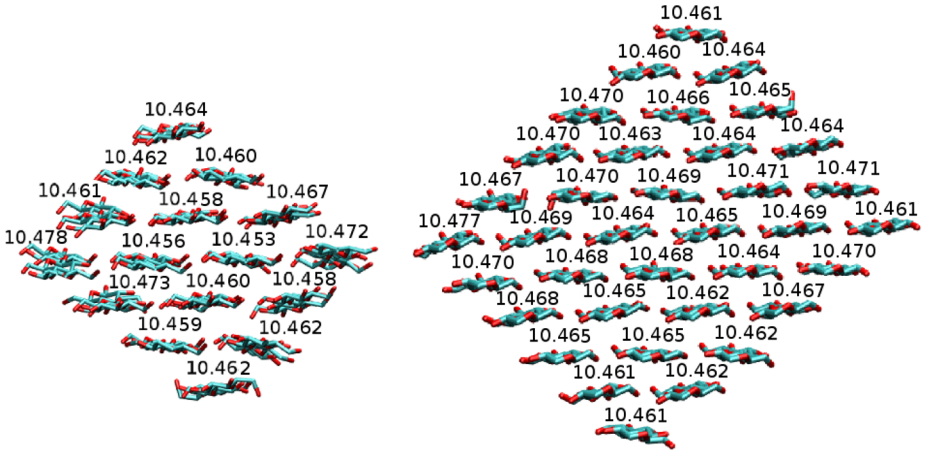

Figure 7. Average unit cellobiose length (Å) for each individual chain of the 4 × 4 and 6 × 6 cellulose microfibrils.

A simple geometrical consideration allows us to compare relative extension of strands in the microfibril core versus those closer to the surface. Figure 7 shows the lengths of the constituent chains within a 4 × 4 and 6 × 6 microfibril, averaged over the last 1 ns of the MD trajectory. The length is measured by averaging the cellobiose length along the glucan chain over time. The case of the 4 × 4 fibril is simple. As expected from the geometry of a simple helix of a given helical angle and distance from the fibril axis, surface chains, which are at a larger distance from the axis, stretch more than interior chains; corner chains stretch the most. The distribution of chain lengths within the 6 × 6 fibril is anisotropic. The length increases as we move from the center to left or right fibril corners shown in Figure 7 and decreases as we move toward the top or bottom corners. Thus, the two distinct types of corners in the diagonal microfibril behave differently: those with neighbors in the same layer—which should be more strongly bound to the remainder of the crystalline fibril—stretch more than those without such neighbors. Geometrically, the first type of chain is located further from the fibril axis than the second. Since the corner chains without in-layer neighbors have relatively weak interchain interactions, they experience larger fluctuations (as demonstrated by Figure 4b). Overall, the accumulation of shear stress across the microfibril cross section due to twist could be relieved only through a loss of crystalline registry between neighboring strands in the microfibril. Several possible modes of relaxation can be envisioned, the softest of which most likely involves rearrangement of chain positions within a cross section (i.e., outer chains becoming inner chains and vice versa, to equalize chain lengths), which could explain observations of axially periodic but narrow amorphous regions that presumably extend across the full width of the microfibril.[57] The effects of shear stress due to increases in microfibril diameter would become visible first at the least bound surface/corner chains, contributing to surface amorphization. Alternative explanations of periodic amorphous regions could involve a deviation from synchronicity of the different subunits of a cellulose synthesis complex.

3.1.3. Local Structure of Twisted Cellulose Microfibril. A *uniform* intrinsic tendency to chirality arising from collective interchain interactions requires that the local interchain bonding geometry be consistent along and across the fibril. Both MD simulation[46−53] and X-ray fiber diffraction[10,68] show hydrogen bonds from the proton on the O3 secondary alcohol group to the O5 ring oxygen of a neighboring residue along the backbone. The O2 secondary alcohol and O6 hydroxymethyl groups are involved in both intrachain hydrogen bonds and interchain hydrogen bonds within the sheets. The hydrogen bond patterns in our MD simulations, shown in Figure 8 and

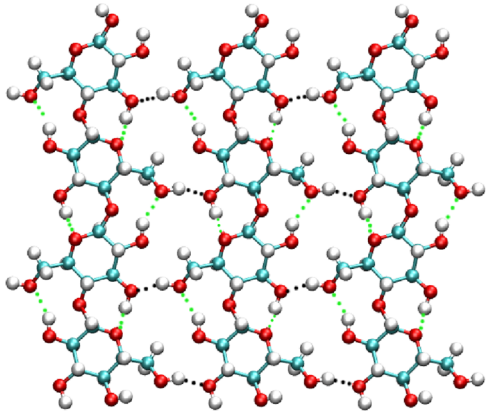

Figure 8. Dominant hydrogen bond pattern suggested by Y. Nishiyama et al.[10] Intrachain hydrogen bonds (O3−H···O5 and O2−H···O6) are indicated by green dots. Interchain hydrogen bonds (O6−H···O3) are indicated by black dots.

Table 2, agree with these observations. We find the (O3)H···O5 distance in MD simulations ranges from 1.7 to 1.8 Å for both origin and center chains for various $n \times n$ microfibrils, in excellent agreement with values (1.7−1.9 Å) derived from X-ray diffraction.[10] Excellent agreements are also observed for (O2)H···O6 and (O6)H···O3 distances. The H-bond parameters obtained from our MD simulations are largely homogeneous regardless of the type of chain (e.g., center or origin chain) and the cross-sectional size. In contrast, the X-ray diffraction study suggested a heterogeneous distribution for the parameters (e.g., 1.966 Å for the origin chain (O3)H···O5 and 1.752 Å for the center chain). This result indicates that a twisted microfibril in MD simulation has a more homogeneous structure. Also, we find consistent bonding patterns at different locations within the same fibril. These results confirm that the hydrogen bonding patterns remain largely consistent across our various fibrils. Thus, all microfibrils sustain the interstrand registry necessary for coherent accumulation of the intrinsic chiral contribution to the energetics.

dx.doi.org/10.1021/jp3089929 | J. Phys. Chem. A 2013, 117, 2580−2589

Table 2. Average Structural Parameters for Cellulose Iβ Microfibrils with Different Cross-Sectional Area from MD Simulations Compared with Experimental Values

	X-ray[10]	3 × 3 model	4 × 4 model	6 × 6 model
		Origin Chains		
(O3)H···O5 (Å)	1.966	1.74 ± 0.15	1.77 ± 0.13	1.77 ± 0.13
(O2)H···O6 (Å)	1.832	2.11 ± 0.53	1.96 ± 0.13	1.96 ± 0.13
(O6)H···O3 (Å)	2.04	2.20 ± 0.29	1.96 ± 0.12	1.97 ± 0.14
O3···O5 (Å)	2.764	2.66 ± 0.07	2.69 ± 0.08	2.67 ± 0.07
O2···O6 (Å)	2.765	3.15 ± 0.39	2.92 ± 0.13	2.89 ± 0.14
O3···O6 (Å)	2.892	3.06 ± 0.20	2.85 ± 0.10	2.84 ± 0.09
φ O5−C1−O4−C4 (deg)	−98.5	−88.2 ± 8.8	−91.4 ± 5.2	−90.5 ± 5.7
ψ C1−O4−C4−C5 (deg)	−142.3	−149.3 ± 7.3	−150.8 ± 6.0	−150.4 ± 5.0
ω1 O5−C5−C6−O6 (deg)	170	167 ± 9	167 ± 8	166 ± 8
ω2 C4−C5−C6−O6 (deg)	−70	−75 ± 8	−75 ± 7	−73 ± 7
		Center Chains		
(O3)H···O5 (Å)	1.752	1.77 ± 0.18	1.71 ± 0.10	1.72 ± 0.09
(O2)H···O6 (Å)	1.904	1.95 ± 0.11	1.92 ± 0.13	1.95 ± 0.12
(O6)H···O3 (Å)	1.779	2.03 ± 0.17	2.17 ± 0.17	2.06 ± 0.13
O3···O5 (Å)	2.705	2.67 ± 0.11	2.65 ± 0.13	2.67 ± 0.09
O2···O6 (Å)	2.865	2.88 ± 0.11	2.86 ± 0.13	2.88 ± 0.13
O3···O6 (Å)	2.711	2.90 ± 0.13	3.03 ± 0.12	2.95 ± 0.11
φ O5−C1−O4−C4 (deg)	−88.7	−89.3 ± 5.3	−91.6 ± 7.4	−91.5 ± 5.3
ψ C1−O4−C4−C5 (deg)	−147.1	−148.9 ± 6.0	−148.0 ± 4.7	−148.6 ± 5.9
ω1 O5−C5−C6−O6 (deg)	158	171 ± 12	171 ± 11	171 ± 10
ω2 C4−C5−C6−O6 (deg)	−83	−69 ± 9	−71 ± 10	−69 ± 10

Table 2 also lists dihedral angles for the glycosidic linkages (φ and ψ) and the hydroxymethyl group (ω1 and ω2). This primary alcohol group has three low-energy conformations (*TG*, *GG*, and *GT*, Figure 9), named according to trans (*T*) or gauche (*G*) dihedral relationships with the ring oxygen O5−C5−C6−O6 (first letter, ω1) and C4−C5−C6−O6 (second letter, ω2). For a glucose molecule in aqueous solution or a vacuum, the *GT* rotamer is most populated, with *GG* slightly less and *TG* the least populated.[69] However, the crystalline environment of cellulose prefers the *TG* conformation because it allows the intrachain O6−O2 hydrogen bond. The average ω1 ranges from 166 to 168° for the origin chain and 171° for the center chain for various microfibril models, which implies that the *TG* rotamer is the most favored conformation, in good agreement with the X-ray studies. Similar to the H-bonding parameters, we find the hydroxymethyl group orientation in our MD simulation is more homogeneous for center and origin chains, a 5° difference compared with a 12° difference in ω value for the center and origin chains in the X-ray studies. Conformational parameters across the glycosidic linkage of origin chains (φ(O5−C1−O4−C4) and ψ(C1−O4−C4−C5)) are also relatively uniform across the 3 × 3, 4 × 4, and 6 × 6 microfibrils (Table 2). Again, the narrowest microfibril, 2 × 2, shows a larger deviation due to surface effects and its data are not listed in Table 2. The root-mean-square fluctuations for φ and ψ range from 6 to 9° for all microfibrils, and they agree relatively well with the experimental data. However, while X-ray diffraction reveals ∼10° differences in both φ and ψ between origin and center chains, their differences are within fluctuations in MD simulation—another indication of the uniformity of glucan chains in a cellulose microfibril.

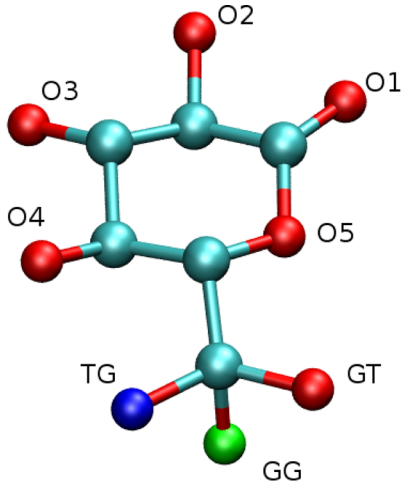

Figure 9. Three low energy orientations (TG, GG, and GT) of the primary alcohol group of β-D-glucose. Hydrogen atoms are omitted for clarity.

3.2. Mechanism for Microfibril Twist. A nonzero helical angle implies some intrinsic chiral contribution to the free energy, which presumably is counterbalanced by higher-order elastic stresses which oppose the twist. One can consider two distinct sources for these counterbalancing stresses: extensional stiffness and torsional stiffness. These two mechanisms have different dependences on helical angle (α) and radius (*R*). Our results thus provide a way to distinguish between these two possibilities.

In the first mechanism, relative elongation of glucan chains (along the *c*-axis) located at different distances *R* from the fibril center gives rise to extensional elastic energy per unit length:[65]

$$E_{\text{extensional}} = \frac{E\pi}{6}\left(\frac{\alpha}{2}\right)^4 R^6$$

which is of fourth order in helical angle $\alpha = 2\pi/\Lambda$. Here *E* denotes the extensional modulus and Λ denotes a helical pitch length. This mechanism does not depend on the registry coherence between the neighboring chains. Instead, it only

dx.doi.org/10.1021/jp3089929 | J. Phys. Chem. A 2013, 117, 2580−2589

depends on the extension of the covalent bond between and within the cellobiose units along a given chain (as well as deformations of the weaker intrachain hydrogen bonds shown with green dotted lines in Figure 8). A similar extensional mechanism combined with an intrinsic fiber twist was used to reproduce equilibrium pitch lengths of sickle hemoglobin fibers observed experimentally.[65]

The second mechanism is based on the fibril's torsional stiffness. The twist is due to distortions in a network of supramolecular interactions, which enforce registry coherence of hydrogen bonds between the neighboring glucan chains. These interchain hydrogen bonds are shown with black dotted lines in Figure 8. Elastic energy increases as neighboring chains shear against each another due to an overall twist deformation. Approximating the cellulose microfibril as an elastic beam of circular cross section, classic beam theory predicts the torsional energy per unit length as

$$E_{\text{torsion}} = \frac{G\pi\alpha^2}{4}R^4$$

where G is the shear modulus of the microfibril.

Thus, for a cellulose microfibril with specified values of angle (α), radius (R), and material properties described by extensional modulus (E) and shear modulus (G), a comparison of the two mechanisms will help determine which one predominately counterbalances the microfibril twist. Remember that the energy gained by fulfilling an intrinsic tendency toward twist is linear in α and thus proportional to αA. If the twist is mainly opposed by glucan chain extension, then

$$E_{\text{extensional}} = \frac{(E\pi)}{6}\left(\frac{\alpha}{2}\right)^4 R^6 \propto \alpha A$$

Keeping in mind that $A \propto R^2$, we obtain

$$\alpha^4 A^3 \propto \alpha A$$

Hence, the helical angle is predicted to be inversely proportional to the two-thirds power of the fibril cross-sectional area:

$$\alpha \propto A^{-2/3}$$

Data fitting (details are included in the Supporting Information) clearly indicates this dependence disagrees with the results of the MD simulations.

In the other case, when the intrinsic twist is opposed by the shear stiffness of the fibril, we have a different energy balance:

$$E_{\text{torsion}} = \frac{G\pi\alpha^2}{4}R^4 \propto \alpha A$$

Therefore, we obtain

$$\alpha^2 A^2 \propto A$$

and thus the helical angle is inversely proportional to the fibril cross-sectional area:

$$\alpha \propto A^{-1}$$

This dependence precisely matches the molecular dynamics results of Figure 6. Therefore, we conclude that the torsional stiffness of the fibril, arising predominately from the supramolecular interactions within a crystalline fibril, provides the opposing elastic force to stabilize a finite value of the fibril twist.

To further support that the extension mechanism can be ruled out for the twist, we carried out a series of thought experiments in which the bond stretching energy, k, for C−O bonds on both sides of the glycosidic oxygen was artificially reduced. The softening of both C−O bonds allows an easier extension of the glucan chain. Should the intrinsic fibril twist be balanced by the stretching of glycosidic linkages, the artificial reduction in their stiffness should markedly increase in the helical angle. Our results indicate otherwise (Figure 10).

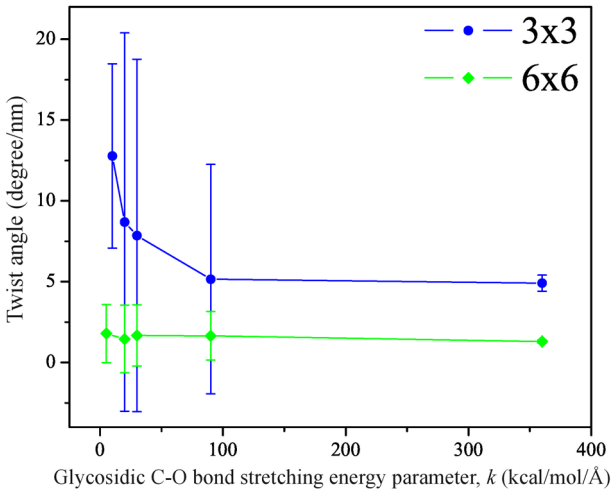

Figure 10. Twist angle of a 3 × 3 cellulose microfibril as a function of the glycosidic C−O bond stretching energy parameter (k). Error bars indicate the fluctuations of the twist angles.

Softening the glycosidic linkage even to 1/3 of its original value does not significantly affect the helical angle. This observation clearly confirms that the extensional stiffness is not the leading mechanism for counterbalancing the intrinsic microfibril twist. If the C−O bond stiffness is still further reduced to extremely small values (the lowest three points of Figure 10), then there is a modest increase in the helical angle for the narrower fibril, but this effect can be easily accounted for by an indirect reduction in shear stiffness due to the extreme softening of the crystalline lattice in this regime. The extensional softening is also associated with an increase in the fluctuations of the helical angle. The increase is much less significant for the 6 × 6 microfibril (from 1.3 to 1.8°/nm) than for the 3 × 3 microfibril (from to 12.8°/nm), consistent with the larger role of fluctuations in the narrower fibrils.

3.3. Mechanical Properties of Twisted Microfibril.

Since wood is a ubiquitous construction material, knowledge of the mechanical properties of cellulose, the most abundant constituent in a plant cell wall, is of great importance. Figure 6 also allows us to calculate some mechanics properties of the cellulose microfibril. If we assume that each constituent chiral glucan chain within a microfibril imposes an intrinsic torque τ on the fibril as a whole, then the total torque T imposed by N chains is $T = \tau N = \sigma A$, corresponding to an areal torque density σ in a microfibril of cross-sectional area A. On physical grounds, σ should have the same value for every fibril, since it originates from the intrinsic chirality of the cellulose unit cell. According to classic beam theory for a continuum model, a circular beam yields a helical angle of $\alpha = T/(GJ)$, where G is the shear modulus and $J = A^2/2\pi$ is the polar area moment. Therefore,

$$\alpha\frac{T}{GJ} = \frac{\sigma A}{G(A^2/2\pi)} = \frac{2\pi\sigma}{G}A^{-1}$$

dx.doi.org/10.1021/jp3089929 | J. Phys. Chem. A 2013, 117, 2580−2589

Dividing the cross-sectional area of the crystalline unit cell by the number of chains that penetrate this cell, we obtain the cross-sectional area of a single microfibril chain as 0.32 nm^2. Together with the slope extracted from the α vs A^{-1} straight line in Figure 6 (with the 2 × 2 microfibril excluded), we can calculate the ratio of the areal torque density to the shear strength: σ/G = 0.045 nm. The precise value of this ratio, and hence the equilibrium helical angles for microfibrils of a given diameter, might depend on the details of the empirical potential used in the molecular dynamics, but the dependence of helical angle on inverse cross-sectional area should be generic across all models that contain a uniform intrinsic torque.

Vertical error bars in Figure 6 show root-mean-square fluctuations ($\Delta\alpha$) in the helical angle across the central region of the microfibril. Since these fluctuations arise from thermal energy resident in elastic torsional modes, their magnitude allows us to estimate the torsional rigidity (C) and shear modulus (G) of the fibril. Equipartition of energy implies that fluctuations of the elastic energy equate to the thermal energy $1/2k_BT$:

$$\frac{C}{2}(\Delta\alpha)^2 L = \frac{1}{2}k_B T$$

where k_B is the Boltzmann constant and L is the length of the microfibril. Recalling that $C = GJ$ and $J = A^2/2\pi$, we obtain

$$\frac{GA^2/2\pi}{2}(\Delta\alpha)^2 L = \frac{1}{2}k_B T$$

and

$$\Delta\alpha = \sqrt{\frac{2\pi k_B T}{GL}}A^{-1}$$

Our simulation results confirm that $\Delta\alpha$ scales linearly with A^{-1}. This well-defined linear dependence allows us to extract a shear modulus of G = 1.6 GPa and a torsional rigidity of $C = 7.3 \times 10^{-26}$ J m. With the value of shear modulus in hand, as well as the σ/G (=0.045 nm) obtained earlier, we are able to calculate the intrinsic areal torque density σ = 0.072 Pa m. This value reflects not simply a torque imposed on a sugar residue by its neighbors along the chain backbone but also a collective effect of supramolecular interactions (i.e., hydrogen bonding, van der Waals, steric repulsion) among all neighbors in the fibril. The estimated shear modulus—in the azimuthal direction—is almost 2 orders of magnitude smaller than previously reported values of the extensional modulus[66] in the axial direction, as would be expected for a strongly anisotropic medium. The microfibril's integrity with respect to axial extension is provided by strong covalent bonds, whereas shearing of neighboring chains involves much weaker noncovalent interactions. Note that the shear modulus calculated here is much larger than the value (G = 0.261 MPa) obtained for sickle hemoglobin fibers.[67] This fact may reflect different mechanisms for the accumulation of the elastic stress under torsion. Not having a strong hydrogen interchain network as in cellulose microfibrils, sickle hemoglobin fibers might adopt the extensional mode as the dominant mechanism of stress accumulation.

With values for various mechanical properties at hand, we can estimate the relative role of the two stabilization mechanisms described in the last section. We find that

$$E_{\text{extensional}} = \frac{E}{6\pi^2}\left(\frac{\alpha}{2}\right)^4 A^3 = 6.2 \times 10^{-14}\ \text{J/m}$$

and

$$E_{\text{torsion}} = \frac{G\alpha^2}{4\pi}A^2 = 8.5 \times 10^{-12}\ \text{J/m}$$

for the 6 × 6 microfibril with α = 1.3°/nm, A = 11.41 nm^2, using a shear modulus of G = 1.6 GPa, and an extensional modulus of E = 150 GPa.[65] This result confirms that the torsional mode of stress accumulation is the dominant mechanism to counterbalance intrinsic twist in the simulated cellulose microfibrils.

The value of the shear modulus G obtained above can be compared to the shear strength (g) values extracted directly from MD simulations. To obtain a rough estimate of g, we slide one glucan chain in the c-direction with respect to a neighboring chain along only one side, as shown in Figure 11. This crude simulation provides a low boundary for g, since

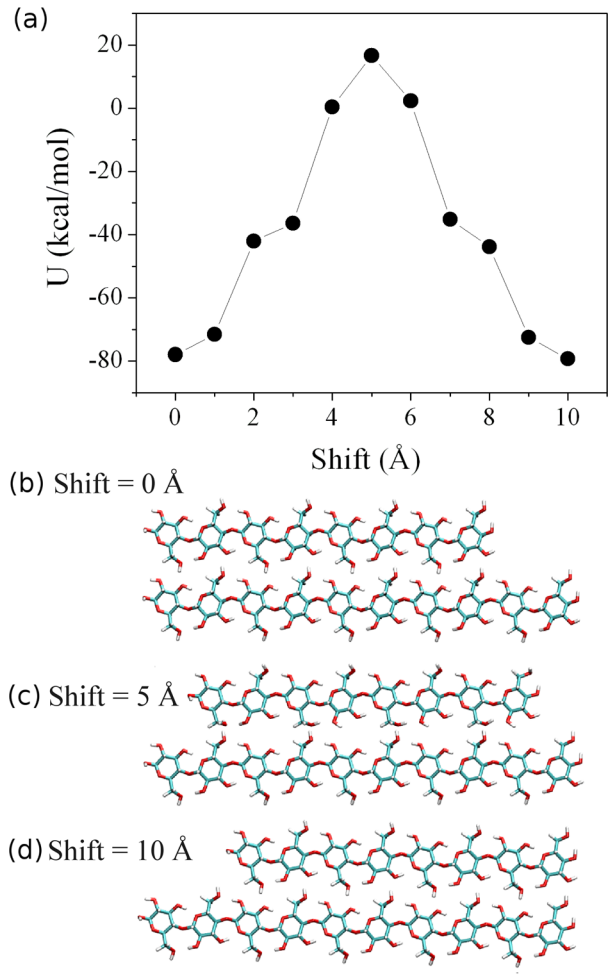

Figure 11. (a) Potential energy (U) as a function of the lateral shift between two glucan chains in the same layer. (b–d) Three representative configurations (shift = 0, 5, and 10 Å) after energy minimization.

we include only one nearest-neighbor contact interaction. Fitting the interaction potential energy with a cosine function, we extract the force (f) required to shift one glucan chain over 5 Å with respect to the neighboring chain from the minimum to the maximum of the sinusoidal dependence ($\Delta E \approx 95$ kcal/mol). Estimating the area of chain contact as $S = xl$, with $x \approx a/2$ and the length of 8 sugar residues $l \approx 40$ Å, we obtain $g \sim f/S$

dx.doi.org/10.1021/jp3089929 | J. Phys. Chem. A 2013, 117, 2580–2589

≈ 1.2 GPa. It is worthwhile to note that this value is comparable (to within the accuracy of this crude estimate of shear stiffness) to the value of G (1.6 GPa) estimated above from the analysis of helical angle fluctuations. Both values are slightly lower than the 1.8−3.8 GPa range reported experimentally.[70]

The intrafibril strain accumulated by persistent helical twist can only be relieved by a disruption of crystallinity sufficiently dramatic that the length difference between inner and outer chains can be corrected (i.e., either an extra glucan subunit must be inserted into the exterior chains or the chains must exchange radial positions within the fibril). Essentially, the microfibril must amorphize across its diameter in order to release the radial extensional shear. The question then becomes: does the energetic gain of relaxing the shear strain exceed the energetic cost of disrupting crystallinity? In other words, does the microfibril pay this cost and find a means to relax the helicity-induced extensional shear, or does it remain in a homogeneously twisted state? Along these lines, periodic amorphous regions, roughly four to five residues long for every ∼300 glucose residues (i.e., ∼150 nm) along the axis, were observed in neutron diffraction experiments of deuterated ramie fiber.[13,57] The periodic crystalline region was found to be much shorter (∼30 nm) in a recent study.[71] Nevertheless, all of these experiments suggested periodic amorphous regions along the axis. Should microfibril twist be a real feature of the microfibril (and not simply an artifact of the empirical potentials used in the molecular dynamics), then it can provide a natural explanation for short regions of fully disrupted crystallinity regularly spaced along the axis of a cellulose microfibril.

The wider microfibrils twist more slowly than narrower microfibrils, proportional to their inverse cross-sectional area. However, the relative slip from center to surface at a given helical angle varies oppositely, proportional to the microfibril width. Combining these two effects, we can deduce that slip from center-to-edge chains (or between neighboring chains) accumulates more slowly in wider microfibrils. Longer axial distances should be required in wider fibrils to reach a particular accumulated length mismatch between different chains. More quantitatively, a chain located at distance R from the axis of a fibril with helical angle α has a length $L(R) \approx L_0(1 + \alpha^2R^2)$. The difference in length between neighboring chains will exceed a critical length ΔL (on the order of a hydrogen bond dimension) over an axial distance of approximately

$$L_0 = \frac{\Delta L(A/\pi)^{3/2}}{4d(\sigma/G)^2}$$

where $\alpha = 2\sigma/(GR_2)$ and d is the radial distance between neighboring chains. Assuming a critical slip length $\Delta L \approx 1$ Å, we obtain $L_0 \sim 250$ nm for the 6 × 6 fibril of cross-sectional area $A = 11.41$ nm^2. This admittedly rough estimate is comparable to the ∼150 nm separation between amorphous regions observed experimentally.[57] This discussion is also consistent with an analysis of cellulose microfibril length/width distribution,[72] in which a linear relationship between cellulose microfibril length and width is proposed, if the length in those studies is associated with the axial separation of amorphous regions.

IV. CONCLUSIONS

All-atom MD simulations in explicit water are performed to investigate conformations of cellulose microfibrils of different cross-sectional shapes and cross-sectional areas, and lengths. The microfibril twist is found to be stable in our 10 ns MD simulation, which allows us to study the structure and mechanical properties of cellulose microfibrils when they are in the twisted state. Our data suggests that the magnitude of twist is inversely proportional to the microfibril cross-sectional area but is independent of its length. The analysis of this finding provides evidence that chiral supramolecular interchain interactions, likely dominated by a combination of steric repulsion and hydrogen bonding, produces a distributed intrinsic torque which is counterbalanced by the torsional stiffness of the fibril in the equilibrium twisted state. Some mechanical properties of the cellulose microfibril are derived on the basis of this finding. The twist structure, although subtle, could provide a natural explanation for disordered regions regularly spaced along the fibril axis. Hence, the long-length-scale structural deformations of the cellulose microfibril may shed light on the mechanism of its biosynthesis.

■ ASSOCIATED CONTENT

Supporting Information

The cross section area and twist angle (and its fluctuation) for various cellulose microfibrils are listed in Table S1. Details for the data fitting for $\alpha \propto A^{-1}$ and $\alpha \propto A^{-2/3}$ are also included. This material is available free of charge via the Internet at http://pubs.acs.org.

■ AUTHOR INFORMATION

Corresponding Author

*E-mail: luz4@psu.edu.

Present Address

⊥M.N.A.M.: School of Advanced Sciences, Crystal Growth and Crystallography Division, VIT University, Vellore 632 041, India.

Notes

The authors declare no competing financial interest.

■ ACKNOWLEDGMENTS

We thank Eric Mockensturm and Paul Lammert for useful discussions. This work is supported as part of The Center for Lignocellulose Structure and Formation, an Energy Frontier Research Center funded by the U.S. Department of Energy, Office of Science, Office of Basic Energy Sciences under Award Number DE-SC0001090. We acknowledge the Penn State University RCC Center for a grant of supercomputer time.

■ REFERENCES

(1) Fernandes, A. N.; Thomas, L. H.; Altaner, C. M.; Callow, P.; Forsyth, V. T.; Apperley, D. C.; Kennedy, C. J.; Jarvis, M. C. *Proc. Natl. Acad. Sci. U.S.A.* **2011**, *108*, E1195−E1203.
(2) Zhang, Y. Z.; Chen, X. L.; Liu, J.; Gao, P. J.; Shi, D. X.; Pang, S. J. *J. Vac. Sci. Technol., B* **1997**, *15*, 1502−1505.
(3) Bailey, A. J.; Brown, R. M. *Ind. Eng. Chem.* **1940**, *32*, 57−63.
(4) Habibi, Y.; Lucia, L. A.; Rojas, O. J. *Chem. Rev.* **2010**, *110*, 3479−3500.
(5) Stockmann, V. E. *Biopolymers* **1972**, *11*, 251−270.
(6) Kratky, O. *Naturwissenschaften* **1942**, *30*, 542−543.
(7) Heyn, A. N. J. *J. Am. Chem. Soc.* **1950**, *72*, 5768−5769.
(8) Heyn, A. N. J. *J. Appl. Phys.* **1955**, *26*, 519−526.

(9) Heikens, D.; Hermans, P. H.; van Velden, P. F.; Weidinger, A. *J. Polym. Sci.* **1953**, *11*, 433−446.
(10) Nishiyama, Y.; Langan, P.; Chanzy, H. *J. Am. Chem. Soc.* **2002**, *124*, 9074−9082.
(11) Nishiyama, Y.; Sugiyama, J.; Chanzy, H.; Langan, P. *J. Am. Chem. Soc.* **2003**, *125*, 14300−14306.
(12) Wada, M.; Heux, L.; Isogai, A.; Nishiyama, Y.; Chanzy, H.; Sugiyama, J. *Macromolecules* **2001**, *34*, 1237−1243.
(13) Wada, M.; Chanzy, H.; Nishiyama, Y.; Langan, P. *Macromolecules* **2004**, *37*, 8548−8555.
(14) Wada, M.; Heux, L.; Nishiyama, Y.; Langan, P. *Cellulose* **2009**, *16*, 943−957.
(15) Langan, P.; Nishiyama, Y.; Chanzy, H. *Biomacromolecules* **2001**, *2*, 410−416.
(16) Langan, P.; Nishiyama, Y.; Chanzy, H. *J. Am. Chem. Soc.* **1999**, *121*, 9940−9946.
(17) French, A. D.; Johnson, G. P. *Cellulose* **2009**, *16*, 959−973.
(18) French, A. D.; Johnson, G. P. *Cellulose* **2004**, *11*, 5−22.
(19) French, A. D.; Johnson, G. P. *Cellulose* **2004**, *11*, 449−462.
(20) Aabloo, A.; French, A. D.; Mikelsaar, R. H.; Pertsin, A. J. *Cellulose* **1994**, *1*, 161−168.
(21) French, A. D.; Johnson, G. P. *Can. J. Chem.* **2006**, *84*, 603−612.
(22) Hanley, S. J.; Revol, J. F.; Godbout, L.; Gray, D. G. *Cellulose* **1997**, *4*, 209−220.
(23) Benziman, M.; Haigler, C. H.; Brown, R. M.; White, A. R.; Cooper, K. M. *Proc. Natl. Acad. Sci. U.S.A.* **1980**, *77*, 6678−6682.
(24) Haigler, C. H.; White, A. R.; Brown, R. M.; Cooper, K. M. *J. Cell Biol.* **1982**, *94*, 64−69.
(25) Brown, R. M., Jr.; Haigler, C. H.; Suttie, J.; White, A. R.; Roberts, E.; Smith, C.; Itoh, T.; Cooper, K. *J. Appl. Polym. Sci.* **1983**, *37*, 33−78.
(26) Bureau, T. E.; Brown, R. M. *Proc. Natl. Acad. Sci. U.S.A.* **1987**, *84*, 6985−6989.
(27) Brown, R., Jr. Microbial cellulose modified during synthesis, US Patent 4942128, 1990.
(28) Okuda, K.; Brown, R. *Protoplasma* **1992**, *168*, 51−63.
(29) Bowling, A. J.; Amano, Y.; Lindstrom, R.; Brown, R. M. *Cellulose* **2001**, *8*, 91−97.
(30) Cannon, R. E.; Anderson, S. M. *Crit. Rev. Microbiol.* **1991**, *17*, 435−447.
(31) Okuda, K.; Tsekos, L.; Brown, R. M. *Protoplasma* **1994**, *180*, 49−58.
(32) Koyama, M.; Helbert, W.; Imai, T.; Sugiyama, J.; Henrissat, B. *Proc. Natl. Acad. Sci. U.S.A.* **1997**, *94*, 9091−9095.
(33) Koyama, M.; Sugiyama, J.; Itoh, T. *Cellulose* **1997**, *4*, 147−160.
(34) Lee, H.; Brown, R. *J. Biotechnol.* **1997**, *57*, 127−136.
(35) Folsom, D. B.; Brown, R. M., Jr. *Physiology of Cell Expansion during Plant Growth*; American Society of Plant Physiologists: Rockville, MD, 1987; pp 58−73.
(36) Brown, R., Jr. *Cellulose and wood: chemistry and technology*; John Wiley and Sons: New York, 1995; pp 639−657.
(37) Haigler, C. H.; Chanzy, H. *J. Ultrastruct. Mol. Struct. Res.* **1988**, *98*, 299−311.
(38) Shibazaki, H.; Kuga, S.; Okano, T. *Cellulose* **1997**, *4*, 75−87.
(39) Kondo, T.; Nojiri, M.; Hishikawa, Y.; Togawa, E.; Romanovicz, D.; Brown, R. M. *Proc. Natl. Acad. Sci. U.S.A.* **2002**, *99*, 14008−14013.
(40) Nobles, D.; Romanovicz, D.; Brown, R., Jr. *Plant Physiol.* **2001**, *127*, 529−542.
(41) Tsekos, I. *J. Phycol.* **1999**, *35*, 635−655.
(42) Colvin, J. *J. Polym. Sci.* **1961**, *49*, 473−477.
(43) Kolpak, F. J.; Blackwell, J. *Text. Res. J.* **1975**, *45*, 568−572.
(44) Preston, R. D. *Polymer* **1962**, *3*, 511−528.
(45) Ruben, G. C.; Bokelman, G. H.; Krakow, W. Plant Cell Wall. Polymers-Biogenesis and Biodegradation. *ACS Symp. Ser.* **1989**, *399*, 278−298.
(46) Nimlos, M. R.; Matthews, J. F.; Crowley, M. F.; Walker, R. C.; Chukkapalli, G.; Brady, J. W.; Adney, W. S.; Cleary, J. M.; Zhong, L.; Himmel, M. E. *Protein Eng., Des. Sel.* **2007**, *20*, 179−187.
(47) Matthews, J. F.; Skopec, C. E.; Mason, P. E.; Zuccato, P.; Torget, R. W.; Sugiyama, J.; Himmel, M. E.; Brady, J. W. *Carbohydr. Res.* **2006**, *341*, 138−152.
(48) Yui, T.; Hayashi, S. *Cellulose* **2009**, *16*, 151−165.
(49) Yui, T.; Hayashi, S. *Biomacromolecules* **2007**, *8*, 817−824.
(50) Yui, T.; Nishimura, S.; Akiba, S.; Hayashi, S. *Carbohydr. Res.* **2006**, *341*, 2521−2530.
(51) Paavilainen, S.; Rog, T.; Vattulainen, I. *J. Phys. Chem. B* **2011**, *115*, 3747−3755.
(52) Matthews, J. F.; Bergenstrahle, M.; Beckham, G. T.; Himmel, M. E.; Nimlos, M. R.; Brady, J. W.; Crowley, M. F. *J. Phys. Chem. B* **2011**, *115*, 2155−2166.
(53) Matthews, J. F.; Beckham, G. T.; Bergenstrahle, M.; Brady, J. W.; Himmel, M. E.; Crowley, M. F. *J. Chem. Theory Comput.* **2012**, *8*, 735−748.
(54) Weisel, J. W.; Nagaswami, C.; Makowski, L. *Proc. Natl. Acad. Sci. U.S.A.* **1987**, *84*, 8991−8995.
(55) Makowski, L.; Magdoff-Fairchild, B. *Science* **1986**, *234*, 1228−1231.
(56) Zhao, L.; Yuan, P.; Liu, N.; Hu, Y.; Zhang, Y.; Wei, G.; Zhou, L.; Zhou, X.; Wang, Y.; Yu, C. *J. Phys. Chem. B* **2009**, *113*, 16178−16183.
(57) Nishiyama, Y.; Kim, U. J.; Kim, D. Y.; Katsumata, K. S.; Roland, P.; Langan, P. *Biomacromolecules* **2003**, *4*, 1013−1017.
(58) Brooks, B. R.; Bruccoleri, R. E.; Olafson, B. D.; Swaminathan, S.; Karplus, M. *J. Comput. Chem.* **1983**, *4*, 187−217.
(59) Guvench, O.; Greene, S. N.; Kamath, G.; Brady, J. W.; Venable, R. M.; Pastor, R. W.; MacKerell, A. D., Jr. *J. Comput. Chem.* **2008**, *29*, 2543−2564.
(60) Guvench, O.; Hatcher, E. R.; Venable, R. M.; Pastor, R. W.; MacKerell, A. D., Jr. *J. Chem. Theory Comput.* **2009**, *5*, 2353−2370.
(61) Jorgensen, W. L.; Chandrasekhar, J.; Madura, J. D.; Impey, R. W.; Klein, M. L. *J. Chem. Phys.* **1983**, *79*, 926−935.
(62) Durell, S. R.; Brooks, B. R.; Ben-Naim, A. *J. Phys. Chem.* **1994**, *98*, 2198−2202.
(63) van Gunsteren, W. F.; Berendsen, H. J. C. *Mol. Phys.* **1977**, *34*, 1311−1327.
(64) Dick-Prez, M.; Zhang, Y.; Hayes, J.; Salazar, A.; Zabotina, O. A.; Hong, M. *Biochemistry* **2011**, *50*, 989−1000.
(65) Turner, M. S.; Briehl, R. W.; Ferrone, F. A.; Josephs, R. *Phys. Rev. Lett.* **2003**, *90*, 128103−128108.
(66) Cintron, M. S.; Johnson, G. P.; French, A. D. *Cellulose* **2001**, *18*, 505−512.
(67) Turner, M. S.; Briehl, R. W.; Wang, J. C.; Ferrone, F. A.; Josephs, J. *J. Mol. Biol.* **2006**, *357*, 1422−1429.
(68) Nishiyama, Y.; Johnson, G. P.; French, A. D.; Forsyth, V. T.; Langan, P. *Biomacromolecules* **2008**, *9*, 3133−3140.
(69) Barnett, C. B.; Naidoo, K. J. *J. Phys. Chem. B* **2008**, *112*, 15450−15459.
(70) Northolt, M. G.; Boerstoel, H.; Maatman, H.; Huisman, R.; Veurink, J.; Elzerman, H. *Polymer* **2001**, *42*, 8249−8264.
(71) Leppanen, K.; Andersson, S.; Torkkeli, M.; Knaapila, M.; Kotelnikova, N.; Serimaa, R. *Cellulose* **2009**, *16*, 999−1015.
(72) Elazzouzi-Hafraoui, S.; Nishiyama, Y.; Putaux, J.; Heux, L.; Dubreuil, F.; Rochas, C. *Biomacromolecules* **2008**, *9*, 57−65.